Crystal structure of a birefringent andradite–grossular from Crowsnest Pass, Alberta, Canada

Sytle M. Antao,[a] and Allison M. Klincker
Department of Geoscience, University of Calgary, Calgary, Alberta T2N 1N4, Canada

(Received 4 August 2013; accepted 16 September 2013)

The structure of a birefringent andradite–grossular sample was refined using single-crystal X-ray diffraction (SCD) and synchrotron high-resolution powder X-ray diffraction (HRPXRD) data. Electron-microprobe results indicate a homogeneous composition of $\{Ca_{2.88}Mn^{2+}_{0.06}Mg_{0.04}Fe^{2+}_{0.03}\}_{\Sigma 3}$ $[Fe^{3+}_{1.29}Al_{0.49}Ti^{4+}_{0.17}Fe^{2+}_{0.06}]_{\Sigma 2}(Si_{2.89}Al_{0.11})_{\Sigma 3}O_{12}$. The Rietveld refinement reduced $\chi^2 = 1.384$ and overall R $(F^2) = 0.0315$. The HRPXRD data show that the sample contains three phases. For phase-1, the weight %, unit-cell parameter (Å), distances (Å), and site occupancy factor (*sof*) are 62.85(7)%, $a = 12.000\,06(2)$, average <Ca–O> = 2.4196, Fe–O = 1.9882(5), Si–O = 1.6542(6) Å, Ca(*sof*) = 0.970(2), Fe(*sof*) = 0.763(1), and Si(*sof*) = 0.954(2). The corresponding data for phase-2 are 19.14(9)%, $a = 12.049\,51(2)$, average <Ca–O> = 2.427, Fe–O = 1.999(1), Si–O = 1.665(1) Å, Ca(*sof*) = 0.928(4), Fe(*sof*) = 0.825(3), and Si(*sof*) = 0.964(4). The corresponding data for phase-3 are 18.01(9)%, $a = 12.019\,68(3)$, average <Ca–O> = 2.424, Fe–O = 1.992(2), Si–O = 1.658(2) Å, Ca(*sof*) = 0.896(5), Fe(*sof*) = 0.754(4), and Si(*sof*) = 0.936(5). The fine-scale coexistence of the three phases causes strain that arises from the unit-cell and bond distances differences, and gives rise to strain-induced birefringence. The results from the SCD are similar to the dominant phase-1 obtained by the HRPXRD, but the SCD misses the minor phases. © *2013 International Centre for Diffraction Data*. [doi:10.1017/S0885715613001255]

Key words: andradite, grossular, birefringence, three-phase intergrowth, Rietveld refinement, HRPXRD, single-crystal X-ray diffraction, electron microprobe

I. INTRODUCTION

Many members of the garnet-group minerals are birefringent. The various reasons given as the cause of the birefringence were recently discussed (Antao and Klincker, 2013). Antao (2013a, 2013b) and Antao and Klincker (2013) proposed a multi-phase intergrowth of slightly different structural (unit-cell and bond distances) and chemical compositions that gives rise to strain, as the only cause of the anisotropy in garnets. This study examines the crystal structure of a birefringent andradite–grossular sample from Crowsnest Pass, southern Alberta. The sample was examined using electron microprobe analyses (EMPA), single-crystal X-ray diffraction (SCD), and high-resolution powder X-ray diffraction (HRPXRD). The EMPA results indicate that the sample is chemically homogeneous, so the multi-phase intergrowths occur on a fine scale. The SCD technique indicates a single-phase sample, but the HRPXRD technique shows a three-phase intergrowth. Such intergrowths cause strain because of structural mismatch, which makes the sample birefringent under cross-polarized light. Preliminary reports were presented (Antao *et al.*, 2013a, 2013b).

Several structure refinements for different garnets in the cubic space group $Ia\bar{3}d$ are available (e.g., Novak and Gibbs, 1971; Basso *et al.*, 1984a, 1984b; Sacerdoti and Passaglia, 1985; Armbruster *et al.*, 1998; Ferro *et al.*, 2003; Adamo *et al.*, 2010). However, the structure for some birefringent garnets was also refined in non-cubic, lower symmetry space groups (e.g., Takéuchi *et al.*, 1982; Nakatsuka *et al.*, 1999; Wildner and Andrut, 2001; Shtukenberg *et al.*, 2005; Frank-Kamenetskaya *et al.*, 2007). Based on the cubic structure refinements of garnet given in the literature, several structural trends across the garnet series were observed (Antao, 2013a, 2013b; see Figure 4).

The general chemical formula for garnet is $^{[8]}X_3\,^{[6]}Y_2\,^{[4]}Z_3\,^{[4]}O_{12}$, $Z = 8$, space group $Ia\bar{3}d$, where the eight-coordinated dodecahedral X site contains Mg, Ca, Mn, or Fe^{2+} cations, the six-coordinated octahedral Y site contains Al, Fe^{3+}, Ti^{4+}, or Zr^{4+} cations, and the four-coordinated tetrahedral Z site contains Si, Fe^{3+}, or Al cations, or (F, O_4H_4) (Novak and Gibbs, 1971; Takéuchi *et al.*, 1982; Smyth *et al.*, 1990; Griffen *et al.*, 1992; Armbruster *et al.*, 1998; Chakhmouradian and McCammon, 2005).

The crystal structure of garnet consists of alternating ZO_4 tetrahedra and YO_6 octahedra with X cations filling the cavities to form the XO_8 dodecahedra. The eight O atoms in the XO_8 polyhedra occur at the corners of a distorted cube (Figure 1). The O atom is bonded to two X, one Y, and one Z in a tetrahedral configuration.

II. EXPERIMENTAL RESULTS

A. Sample characterization

The andradite–grossular sample occurs in an extrusive alkaline igneous complex at Crowsnest Pass, southern Alberta, Canada. The sample was collected on a road cut on highway

[a]Author to whom correspondence should be addressed. Electronic mail: antao@ucalgary.ca.

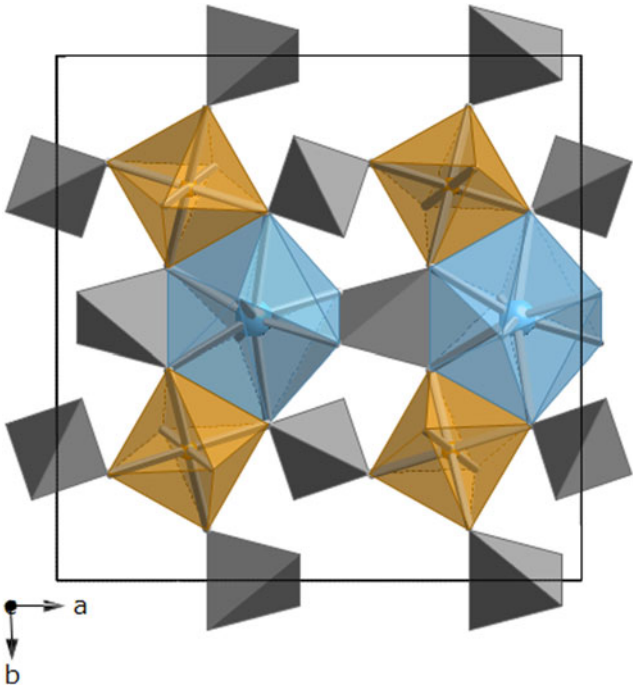

Figure 1. (Color online) Projection of the garnet structure down **c** showing the ZO_4 tetrahedra, YO_6 octahedra, and XO_8 dodecahedra where the eight O atoms occur at the corners of a distorted cube.

3, near the town of Coleman. Phenocrysts of andradite–grossular occur with aegirine-augite, sanidine, analcime, and plagioclase in trachyte and phonolite volcanic flows, agglomerates, and tuffs (Dingwell and Brearley, 1985). Some andradite–grossular crystals are chemically zoned; the Fe and Ti contents decrease from the core to the rim (Hilton, 2000). The euhedral andradite–grossular crystals used in this study are dark brown to black in color, about 4 mm in diameter, and show low birefringence in cross-polarized light (Figure 2). In plain-polarized light, lamellar features are observed [Figure 2(a)]. The sample shows fine-scale tweed-like features [Figure 2(b)].

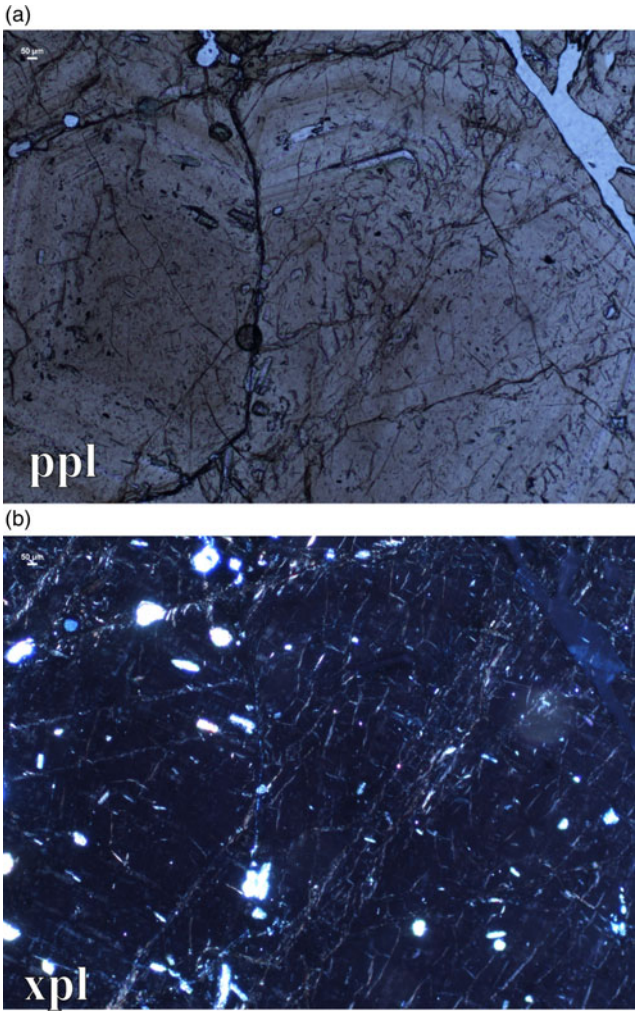

Figure 2. (Color online) Optical microscopy thin-section images for the andradite-grossular from Crowsnest Pass: (a) plane-polarized light (ppl) and (b) cross-polarized light (xpl). The lamellar features are contained in (a). Fine-scale tweed-like features occur in (b). The scale bars represent 50 μm (top left).

B. Electron microprobe analysis

The Crowsnest Pass sample (≈2 mm in diameter) was analyzed by using a JEOL JXA-8200 WD-ED electron-microprobe analyzer (EMPA). The JEOL operating program on a Solaris platform was used for ZAF correction and data reduction. The wavelength-dispersive operating conditions were 15 kV accelerating voltage, 20 nA beam current, and a beam diameter of 5 μm. Various minerals were used as standards [*e.g.*, almandine-pyrope (Mg$K\alpha$), grossular (Ca$K\alpha$), almandine (Fe$K\alpha$, Al$K\alpha$, and Si$K\alpha$), rutile (Ti$K\alpha$), spessartine (Mn$K\alpha$), and chromite (Cr$K\alpha$)]. The sample appears homogeneous based on EMPA data from eight spots from different areas of the crystal (Table I). However, the structure refinement of the three phases shows small variations in their compositions. The intergrowth of the three phases occurs on a fine scale that cannot be resolved by EMPA.

C. Single-crystal X-ray diffraction

A suitable single crystal of andradite–grossular, which may consist of three phases, was selected with a binocular microscope and mounted on a glass fiber for SCD using a Nonius KAPPA APEX II CCD 4-circle X-ray diffractometer equipped with graphite monochromated Mo $K\alpha$ radiation. The intensity data were obtained in the ω–ϕ scanning mode with the goniometer and detector angular settings optimized. The unit-cell parameter and the orientation matrices were obtained by using the entire reflection dataset collected at 23 °C. The diffraction spots were measured in full, scaled with SCALEPACK, corrected for Lorentz-polarization, and integrated using DENZO (Otwinowski and Minor, 1997). The structure was refined with SHELXL-97 using a full-matrix least-squares refinement on F^2 (Sheldrick, 1997; Table II). Scattering curves for neutral atoms were used. Atom positions and equivalent isotropic displacement parameters are given in Table IV, anisotropic displacement parameters are given in Table V, and bond distances are given in Table VI. A list of the observed and calculated structure factors is available as supplemental data (available online at http://www.journals.cambridge.org/PDJ).

D. Synchrotron HRPXRD

The andradite–grossular sample was studied by HRPXRD that was performed at beamline 11-BM, Advanced Photon Source (APS), Argonne National Laboratory (ANL). A small

https://doi.org/10.1017/S0885715613001255 Published online by Cambridge University Press

TABLE I. Electron microprobe analysis[a] of andradite–grossular from Crowsnest Pass, Alberta, Canada.

Oxides	Min.	Max.	Average
SiO_2 (wt.%)	34.13	34.93	34.93(27)
TiO_2	2.71	3.55	2.71(28)
Al_2O_3	5.71	6.57	6.18(35)
Cr_2O_3	0.00	0.03	0.00(1)
FeO_{tot}	19.91	20.15	19.80(25)
Fe_2O_3 (calc)			
MnO	0.76	0.86	0.82(4)
MgO	0.26	0.34	0.34(3)
CaO	29.86	32.54	32.48(94)
$\sum$			97.25
Recalculated (wt.%)			
Final FeO			1.17(1.23)
Final Fe_2O_3			20.70(1.47)
$\sum$(calc)			99.32
Cations for 12 O atoms			
Mn^{2+}			0.057(2)
Mg^{2+}			0.042(3)
Ca^{2+}			2.876(49)
$\sum X$			3.000
Ti^{4+}			0.169(20)
Al^{3+}			0.488(37)
Cr^{3+}			0.000(1)
Fe^{2+}			0.055(40)
Fe^{3+}			1.288(79)
$\sum Y$			2.000
Si^{4+}			2.887(22)
Al^{3+}			0.113(22)
$\sum Z$			3.000
End-member mole %			
Schorlomite-Al			**5.67**
Morimotoite			**5.53**
Spessartine (Sps)			1.91
Pyrope (Prp)			1.38
Almandine (Alm)			0.85
Grossular (Grs)			**20.27**
Andradite (Adr)			**64.38**
$\sum$			99.99
Quality index			Superior

EMPA data were analyzed by using the spreadsheet from Locock (2008). The estimated standard deviation in brackets is based on the average analyses from eight spots. Numbers in bold indicate significant end-members.

fragment (≈2 mm in diameter) of the sample was crushed to a fine powder (<10 μm in diameter) using an agate mortar and pestle. The crushed sample was loaded into a Kapton capillary (0.8-mm internal diameter) and rotated during the experiment at a rate of 90 rotations per second. The data were collected at 23 °C to a maximum 2θ of about 50° with a step size of 0.001° and a step time of 0.1 s per step. The HRPXRD trace was collected with twelve silicon (111) crystal analyzers that increase detector efficiency, reduce the angular range to be scanned, and allow rapid acquisition of data. A silicon (NIST 640c) and alumina (NIST 676a) standard (ratio of ⅓ Si : ⅔ Al_2O_3 by weight) was used to calibrate the instrument and refine the monochromatic wavelength used in the experiment (Table III). Additional details of the experimental setup are given elsewhere (Antao *et al.*, 2008; Lee *et al.*, 2008; Wang *et al.*, 2008).

E. Rietveld structure refinement

The HRPXRD data were analyzed by the Rietveld method (Rietveld, 1969), as implemented in the *GSAS* program (Larson and Von Dreele, 2000), and using the *EXPGUI* interface (Toby, 2001). Scattering curves for neutral atoms were used. The starting atom coordinates, unit-cell parameter, and space group $Ia\bar{3}d$, were taken from Antao and Klincker (2013). The background was modeled using a Chebyschev polynomial (5 terms). The reflection-peak profiles were fitted using type-3 profile (pseudo-Voigt function with the asymmetrical model; Finger *et al.*, 1994) in the *GSAS* program. A full-matrix least-squares refinement was conducted by varying the parameters in the following sequence: a scale factor, unit-cell parameter, atom coordinates, and isotropic displacement parameters. Examination of the HRPXRD trace for andradite–grossular clearly shows the presence of three separate phases with different cubic unit-cell parameters (Figure 3). The three separate phases were refined together with the site occupancy factors (*sofs*) in terms of Ca, Fe, and Si atoms in the X, Y, and Z sites, respectively. Toward the end of the refinement, all of the parameters were allowed to vary simultaneously, and the refinement proceeded to convergence. The fitted HRPXRD trace for the three-phase refinement is shown (Figure 3).

The unit-cell parameters and the Rietveld refinement statistics for the three cubic phases in the andradite–grossular sample are listed in Table III. The atom coordinates, isotropic displacement parameters, and *sofs* are given in Table IV. Bond distances and angles are given in Table VI.

TABLE II. Single-crystal (SCD) data for andradite–grossular.

Temperature	293(1) K
Wavelength	0.710 73 Å
Unit-cell parameter	$a = 11.9930(9)$ Å
Absorption coefficient	5.6 mm^{-1}
Crystal size	$0.05 \times 0.05 \times 0.05$ mm^3
θ range for data collection	4.16 to 27.20°
Limiting indices	$-15 \le h \le 15$, $-15 \le k \le 15$, $-15 \le l \le 15$
Reflections collected/unique	3070/166 [R(int) = 0.077]
Completeness to $\theta = 27.20$	100.0%
Absorption correction	None
Refinement method	Full-matrix least-squares on F^2
Data/restraints/parameters	166/0/21
Goodness-of-fit on F^2	1.227
Final R indices [$I>2\sigma(I)$]	$R_1 = 0.0331$, w$R_2 = 0.0469$
R indices (all of the data)	$R_1 = 0.0441$, w$R_2 = 0.0501$
Largest diff. peak and hole	0.311 and −0.259 e/A^3

https://doi.org/10.1017/S0885715613001255 Published online by Cambridge University Press

TABLE III. HRPXRD data and Rietveld refinement statistics for andradite-grossular.

	Phase-1	Phase-2	Phase-3
wt. %	62.85(7)	19.14(9)	18.01(9)
[a]LY	12.4(1)	12.7(1)	11.3(1)
a (Å)	12.000 06(2)	12.049 51(2)	12.019 68(3)
[b]Δa (Å)	–	−0.0495	−0.0196
Reduced χ^2	1.195		
[c]R (F^2)	0.0313		
λ (Å)	0.424 65(2)		
2θ range (°)	2 to 50		
Data points	47 997		
N_{obs}	1948		

[a]LY is related to the strain and these values are quite large compared to a single-phase grossular from Montana, where LY = 5.0(1) (Antao, 2013a).
[b]Based on thin film, both the strain and birefringence between the substrate and film are proportional to $\Delta a = (a_{substrate} - a_{film})$ (Kitamura and Komatsu, 1978).
[c]Overall R (F^2) = R-structure factor based on observed and calculated structure amplitudes = $[\sum(F_o^2 - F_c^2)/\sum(F_o^2)]^{1/2}$.

III. DISCUSSION

The andradite–grossular sample has a composition, $\{Ca_{2.88}Mn^{2+}_{0.06}Mg_{0.04}Fe^{2+}_{0.03}\}_{\Sigma3}[Fe^{3+}_{1.29}Al_{0.49}Ti^{4+}_{0.17}Fe^{2+}_{0.06}]_{\Sigma2}(Si_{2.89}Al_{0.11})_{\Sigma3}O_{12} \approx Adr_{64}Grs_{20}$, with Ca^{2+}, Fe^{3+}, and Si^{4+} as dominant cations in the X, Y, and Z sites, respectively (Table I). The distribution of the cations is indicated by the chemical formula. The EMPA results indicate a homogeneous composition because the intergrowth of the three cubic phases occurs on a fine scale that cannot be resolved by EMPA.

The HRPXRD trace for andradite–grossular clearly shows the presence of three cubic phases within the sample (Figure 3). The crystal structure of the three cubic phases was modeled quite well, as indicated by the reduced χ^2 and overall R (F^2) Rietveld refinement values of 1.384 and 0.0315, respectively (Table III). Splitting of the reflections for different members of the garnet group, as shown in Figure 3, is known but its significance was not fully evaluated. For example, Koritnig *et al.* (1978) reported splitting of the diffraction peaks in garnet, which is inconsistent with cubic symmetry. Splitting of the diffraction peaks was also observed by Lager *et al.* (1989) for a synthetic deuterated hibschite garnet, and they used multiple-phase (four cubic phases) Rietveld refinement to analyze their neutron-diffraction data. Splitting of garnet reflections was also reported in several studies that examine high-pressure and high-temperature garnet phases (e.g., Ganguly *et al.*, 1993; Parise *et al.*, 1996; Heinemann *et al.*, 1997).

The bond distances for the three phases compare well with the other published structures (Figure 4). The a unit-cell parameters for phase-1, -2, and -3 for the Crowsnest Pass andradite–grossular are 12.000 06(2), 12.049 51(2), and 12.019 68 (3) Å, respectively, and their corresponding weight % are 62.85(7), 19.14(9), and 18.01(9) (Table III). Hilton (2010) reported a unit-cell parameter of 12.0249 Å for an andradite–grossular sample from the same general locality. The unit-cell parameters are slightly different for the three phases, but they are between the values for uvarovite and andradite (Figure 4). It is interesting to note that this sample contains

TABLE IV. Atom coordinates[a], and isotropic displacement parameters (Å^2), and sofs for andradite–grossular.

Method		SCD	HRPXRD		
Phase		Single phase	Phase-1	Phase-2	Phase-3
Ca(X)	*U*	0.009(1)	0.0068(1)	0.0050(3)	0.0048(3)
Fe/Al(Y)	*U*	0.005(1)	0.003 46(7)	0.0029(1)	0.0030(2)
Si(Z)	*U*	0.006(1)	0.0047(2)	0.0059(4)	0.0067(5)
O	*x*	0.0382(2)	0.038 20(5)	0.038 49(9)	0.0384(1)
	y	0.0481(2)	0.047 56(4)	0.048 62(9)	0.0480(1)
	z	0.6541(2)	0.654 05(4)	0.653 88(9)	0.6539(1)
	U	0.011(1)	0.0110(2)	0.0127(4)	0.0167(6)
Ca(X)	*sof*	0.982(3)	0.970(2)	0.928(4)	0.896(5)
Fe(Y)	*sof*	0.768(2)	0.763(1)	0.825(3)	0.754(4)
Si(Z)	*sof*	0.945(3)	0.954(2)	0.964(4)	0.936(5)
Ca(X)	*EMPA sof*	1.002(5)			
Fe(Y)	*EMPA sof*	0.865(10)			
Si(Z)	*EMPA sof*	0.997(1)			
[b]X	*Δ (sof)*	−0.020	−0.032	–	–
Y	*Δ (sof)*	−0.097	−0.102	–	–
Z	*Δ (sof)*	−0.052	−0.043	–	–
[c]X	*Δ e*	−0.40	−0.64	–	–
Y	*Δ e*	−2.52	−2.65	–	–
Z	*Δ e*	−0.73	−0.60	–	–

[a]X is at (0, ¼, and ⅛), Y at (0, 0, and 0), and Z at ((⅜, 0, and ¼). For the SCD, U_{eq}. is defined as one third of the trace of the orthogonalized U_{ij} tensor.
[b]Δ(*sof*) = *sof* (refinement) – *sof* (EMPA).
[c]Δe = electrons (refinement) – electrons (EMPA).

https://doi.org/10.1017/S0885715613001255 Published online by Cambridge University Press

TABLE V. Anisotropic displacement parameters (Å^2) obtained by the SCD for andradite–grossular.

	U_{11}	U_{22}	U_{33}	U_{23}	U_{13}	U_{12}
Ca(X)	0.010(1)	0.010(1)	0.006(1)	0	0	0.002(1)
Fe(Y)	0.005(1)	0.005(1)	0.005(1)	0.000(1)	0.000(1)	0.000(1)
Si(Z)	0.006(1)	0.006(1)	0.006(1)	0	0	0
O(1)	0.012(1)	0.010(1)	0.011(2)	0.001(1)	0.002(1)	0.000(1)

Anisotropic displacement factor exponent takes the form: $-2\pi^2[h^2a^{*2}\ U_{11}+\ldots+2hka^*b^*U_{12}]$.

0.17 apfu Ti atoms, but it is not in the Ti-andradite region (Figure 4). Data for the andradite–grossular sample, obtained from the HRPXRD and SCD methods, are shown in Figure 4 and they occur to the left of the end-member andradite, whereas most Ti-rich andradites occur to the right (see Antao, 2013b). Although the sample contains some Ti atoms, it has significant grossular content, so it plots to the left of the end-member andradite (Figure 4).

The *sofs* obtained from the refinement are not exactly the same as those calculated from the EMPA analysis, but their values are similar (Table IV). From the HRPXRD refinement, there is a constant Si atom deficiency of about 5% in the Z site, which may indicate minor $(O_4H_4) \leftrightarrow SiO_4$ substitution because the Si–O distance is nearly constant in the three phases (Figure 4). In calculating the chemical formula, a minor amount of Al is placed in the Si site (Table I). The Ca(*sof*) from the HRPXRD refinement varies from 0.90 to 0.97, hence the average <Ca–O> distance differs by a small amount. The Fe(*sof*) varies from 0.75 to 0.83, hence the Fe–O distance shows minor variations (Figure 4). The formation of the three-phase intergrowth in garnet in Si-deficient rocks may be related to changes in oxygen fugacity (f_{O2}), activity of SiO_2 (a_{SiO2}), etc., as the crystals grow at low temperature that prevents diffusion or homogenization of the sample. Alternatively, the three-phase intergrowth may be the stable form. The intimate contact of the three phases in a crystal causes strain that arises from the structural mismatch and gives rise to the birefringence; similar intergrowths occur in other birefringent garnets (Antao, 2013a, 2013b; Antao and Klincker, 2013). HRPXRD is showing that multi-phase intergrowths are quite common in garnet. The strain in the three cubic phases is about the same because each phase occurs in significant quantity (Table III). Their large strain is significantly more than that for a single cubic phase. The strains that can be calculated from the LY values are not very different from the relative differences in the unit-cell parameters (Table III).

In this study, single-crystal data were collected before HRPXRD data showed that the sample consists of three cubic phases. The single-crystal results for the sample match the dominant phase-1 HRPXRD results (Tables II, III, IV, and VI), but miss the other two minor phases (Figure 3). The unit-cell parameter derived from the SCD is 11.9930(9) Å compared to 12.000 06(2) Å obtained from the HRPXRD, which indicates that the HRPXRD is a superior technique to obtain the unit-cell parameters. Moreover, the SCD data are affected by the two other phases in the sample. Most of the published work on garnet has used the single-crystal method, and probably missed the minor phases in multi-phase samples, especially for those garnets that are birefringent. The single-crystal method is an inappropriate technique to examine multi-phase garnet samples that now appear to be quite common, as is being shown by the HRPXRD data (Antao, 2013a, 2013b; Antao and Klincker, 2013).

Our SCD study shows that reasonable structural data can be obtained from the samples that consist of multiple phases, but such results are misleading because the minor phases are missed (Figure 4). Moreover, many SCD structure refinements using the cubic space group were performed on birefringent garnet samples (e.g., Smyth *et al.*, 1990; Armbruster *et al.*, 1998). Such birefringent samples probably contain multiple phases. It is important to identify the SCD results in the literature that seem to contain multiple phases, instead of accepting the reasons given for unusual structural parameters. In some cases, it is easy to identify samples that may contain multiple phases from the unreasonable anisotropic displacement ellipsoid for the O atom that elongate along the "Si–O" bond, instead at about 90° to the bond (e.g., Armbruster, 1995; Peterson *et al.*, 1995; Ferro *et al.*, 2003). Some other studies may not report or discuss the unusual anisotropic

TABLE VI. Selected distances (Å) for andradite-grossular.

Method		SCD	HRPXRD		
Phase		Single phase	Phase-1	Phase-2	Phase-3
Z–O	x4	1.655(3)	1.6542(6)	1.665(1)	1.658(2)
Y–O	x6	1.989(2)	1.9882(5)	1.999(1)	1.992(2)
X–O	x4	2.343(3)	2.3425(5)	2.359(1)	2.351(2)
X–O	x4	2.490(2)	2.4966(5)	2.495(1)	2.496(2)
<X–O>	[8]	2.417	2.4196	2.427	2.424
*<D–O>		2.119	2.1204	2.130	2.124

These distances are shown in Figure 4 for comparison to published data. For the calculated radii sum distances, radii from Shannon (1976) were used (X site: Mn^{2+} = 0.96, Mg = 0.89, Fe^{2+} = 0.92 Å; Y site: Ti^{4+} = 0.605, Al = 0.535, Fe^{2+} = 0.78, Fe^{3+} = 0.645 Å; Z site: Si = 0.26, Al = 0.39 Å; and O = 1.38 Å). Ca = 1.06 instead of 1.12 Å; this gives more realistic <X–O> distances. *<D–O> = {(Z–O)+(Y–O)+(X–O)+(X′–O)}/4. Based on the EMPA data and the above radii, the radii sum distances are as follows: Z–O = 1.64, Y–O = 2.00, <X–O> = 2.43, and <D–O> = 2.13 Å.

https://doi.org/10.1017/S0885715613001255 Published online by Cambridge University Press

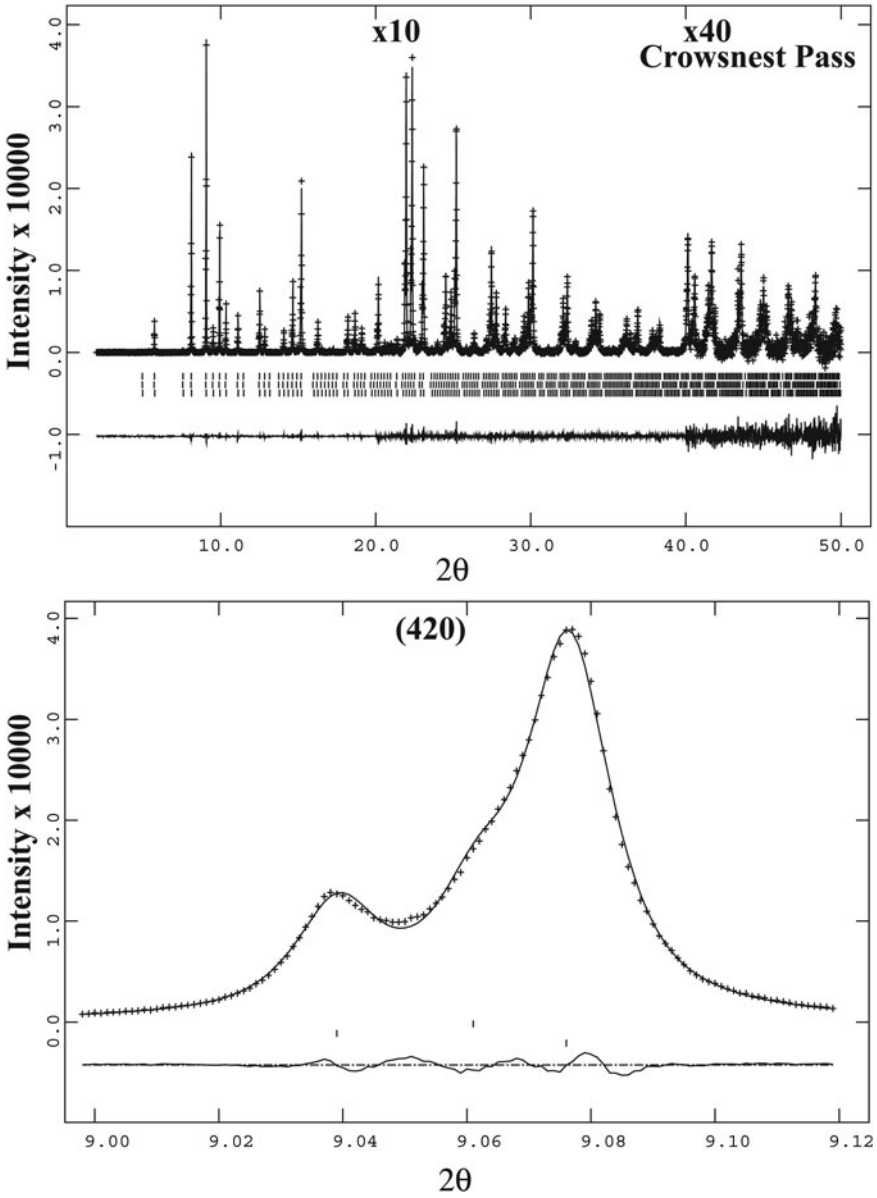

Figure 3. HRPXRD trace for the andradite–grossular from Crowsnest Pass, together with the calculated (continuous line) and observed (crosses) profiles. The difference curve (I_{obs} – I_{calc}) is shown at the bottom. The short vertical lines indicate allowed reflection positions. (a) The intensities for the trace and difference curve that are above 20 and 40° 2θ are scaled by factors of ×10 and ×40, respectively. (b) Peak (420) is displayed as an example to show the three-phase intergrowth.

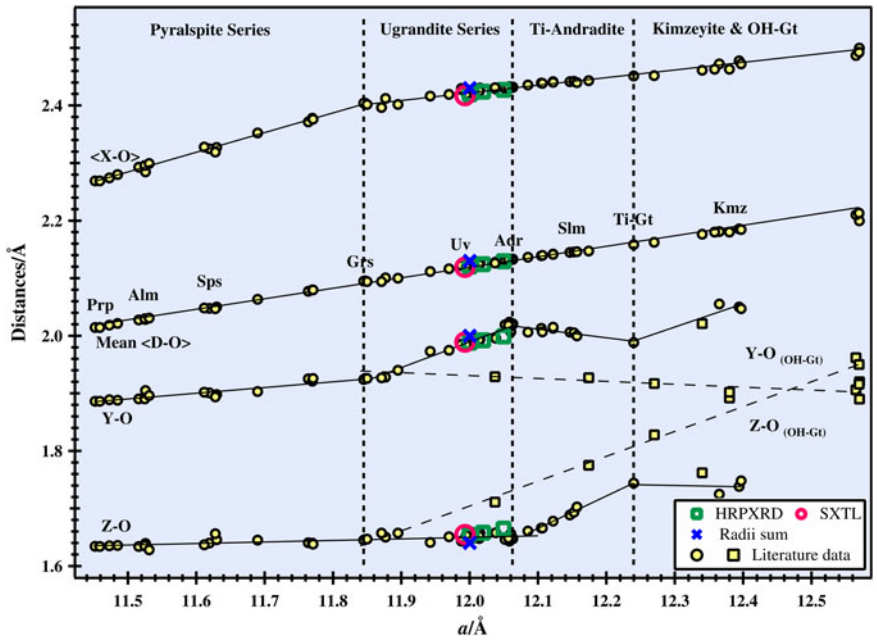

Figure 4. (Color online) Structural variations across the cubic garnet-group minerals. The Y–O, Z–O, and average <X–O> distances in various parts of the series vary linearly with the *a* unit-cell parameter. The mean <D–O> distance varies linearly with the *a*-parameter across the series (Antao, 2013a, 2013b). The literature data (solid yellow circles and squares) are based on cubic refinements of the garnet structure. For the hydrogarnets (yellow squares), Y–O and Z–O trend lines, labeled as OH-Gt, are also shown, but such distances from Armbruster (1995) were not included in the computation of these trend lines because they are way off. The hydrogarnet <X–O> and D–O distances occur on the general trend lines. Data for the andradite–grossular from Crowsnest Pass, obtained from the HRPXRD and SCD methods, are shown to the left of the end-member andradite, whereas most Ti-rich andradites occur to the right (see Antao, 2013b).

https://doi.org/10.1017/S0885715613001255 Published online by Cambridge University Press

displacement parameters, but simply report isotropic values (e.g., Chakhmouradian *et al.*, 2008).

In this study and those by Antao and Klincker (2013) and Antao (2013a, 2013b), a general solution to the birefringence problem in garnet is proposed whereby multi-phase intergrowths result in structural mismatch (different unit-cell parameters and bond distances) that gives rise to strain-induced birefringence. Similar intergrowths also occur in other birefringent garnet samples, whereas isotropic garnet occurs as a single-phase, as in the grossular sample from Montana (Antao, 2013a). Multi-phase intergrowths are not uncommon and were also observed in the helvine-group minerals (Antao and Hassan, 2010) and in apatite (Baikie *et al.*, 2012).

ACKNOWLEDGEMENTS

We thank R. Marr and M. Parvez for help with the EMPA and SCD data collection, respectively. The HRPXRD data were collected at the X-ray Operations and Research beamline 11-BM, Advanced Photon Source (APS), and Argonne National Laboratory (ANL). Use of the APS was supported by the U.S. Dept. of Energy, Office of Science, Office of Basic Energy Sciences, under Contract No. DE-AC02-06CH11357. This work was supported with an NSERC Discovery grant and an Alberta Ingenuity Award to SMA.

SUPPLEMENTARY MATERIALS AND METHODS

The supplementary material for this article can be found at http://www.journals.cambridge.org/PDJ

Adamo, I., Gatta, G. D., Rotitoti, N., Diella, V., and Pavese, A. (**2010**). "Green andradite stones: gemological and mineralogical characterisation," Eur. J. Mineral. **23**, 91–100.

Antao, S. M. (**2013a**). "Three cubic phases intergrown in a birefringent andradite–grossular garnet and their implications," Phys. Chem. Miner. **40**, 705–716.

Antao, S. M. (**2013b**). "The mystery of birefringent garnet: is the symmetry lower than cubic?," Powder Diffr. doi: 10.1017/S0885715613000523.

Antao, S. M. and Hassan, I. (**2010**). "A two-phase intergrowth of genthelvite from Mont Saint-Hilaire, Quebec," Can. Mineral. **48**, 1217–1223.

Antao, S. M. and Klincker, A. M. (**2013**). "Origin of birefringence in andradite from Arizona, Madagascar, and Iran," Phys. Chem. Miner. **40**, 575–586.

Antao, S. M., Hassan, I., Wang, J., Lee, P. L., and Toby, B. H. (**2008**). "State-of-the-art high-resolution powder X-ray diffraction (HRPXRD) illustrated with Rietveld structure refinement of quartz, sodalite, tremolite, and meionite.," Can. Mineral. **46**, 1501–1509.

Antao, S. M., Klincker, A. M., and Round, S. A. (**2013a**). "Origin of birefringence in common silicate garnet: intergrowth of different cubic phases," Am. Geophys. Union Conference, Cancun, Mexico, 14–17 May, 2013.

Antao, S. M., Klincker, A. M., and Round, S. A. (**2013b**). "Some garnets are cubic and birefringent, why?," Conference, Hawaii, USA, 20–24 July, 2013.

Armbruster, T. (**1995**). "Structure refinement of hydrous andradite, $Ca_3Fe_{1.54}Mn_{0.02}Al_{0.26}(SiO_4)_{1.65}(O_4H_4)_{1.35}$, from the Wessels mine, Kalahari manganese field, South Africa," Eur. J. Mineral. **7**, 1221–1225.

Armbruster, T., Birrer, J., Libowitzky, E., and Beran, A. (**1998**). "Crystal chemistry of Ti-bearing andradites," Eur. J. Mineral. **10**, 907–921.

Baikie, T., Schreyer, M. K., Wong, C. L., Pramana, S. S., Klooster, W. T., Ferraris, C., McIntyre, G. J., and White, T. J. (**2012**). "A multi-domain gem-grade Brazilian apatite," Am. Mineral. **97**, 1574–1581.

Basso, R., Cimmino, F., and Messiga, B. (**1984a**). "Crystal chemical and petrological study of hydrogarnets from a Fe-gabbro metarodingite (Gruppo Di Voltri, Western Liguria, Italy)," Neues Jahrbuch Fur Mineralogie-Abhandlungen **150**, 247–258.

Basso, R., Cimmino, F., and Messiga, B. (**1984b**). "Crystal-chemistry of hydrogarnets from three different microstructural sites of a basaltic metarodingite from the Voltri-Massif (Western Liguria, Italy)," Neues Jahrbuch Fur Mineralogie-Abhandlungen **148**, 246–258.

Chakhmouradian, A. R. and McCammon, C. A. (**2005**). "Schorlomite: a discussion of the crystal chemistry, formula, and inter-species boundaries," Phys. Chem. Miner. **32**, 277–289.

Chakhmouradian, A. R., Cooper, M. A., Medici, L., Hawthorne, F. C., and Adar, F. (**2008**). "Fluorine-rich hibschite from silicocarbonatite, Afrikanda complex, Russia: crystal chemistry and conditions of crystallization," Can. Mineral. **46**, 1033–1042.

Dingwell, D. B. and Brearley, M. (**1985**). "Mineral chemistry of igneous melanite garnets from analcite-bearing volcanic rocks, Alberta, Canada," Contrib. Mineral. Petrol. **90**, 29–35.

Ferro, O., Galli, E., Papp, G., Quartieri, S., Szakall, S., and Vezzalini, G. (**2003**). "A new occurrence of katoite and re-examination of the hydrogrossular group," Eur. J. Mineral. **15**, 419–426.

Finger, L. W., Cox, D. E., and Jephcoat, A. P. (**1994**). "A correction for powder diffraction peak asymmetry due to axial divergence," J. Appl. Crystall. **27**, 892–900.

Frank-Kamenetskaya, O. V., Rozhdestvenskaya, L. V., Shtukenberg, A. G., Bannova, I. I., and Skalkina, Y. A. (**2007**). "Dissymmetrization of crystal structures of grossular–andradite garnets $Ca_3(Al, Fe)_2(SiO_4)_3$," Struct. Chem. **18**, 493–503.

Ganguly, J., Cheng, W., and O'Neill, H. S. C. (**1993**). "Syntheses, volume, and structural changes of garnets in the pyrope–grossular join: implications for stability and mixing properties," Am. Mineral. **78**, 583–593.

Griffen, D. T., Hatch, D. M., Phillips, W. R., and Kulaksiz, S. (**1992**). "Crystal chemistry and symmetry of a birefringent tetragonal pyralspite$_{75}$-grandite$_{25}$ garnet," Am. Mineral. **77**, 399–406.

Heinemann, S., Sharp, T. G., Seifert, F., and Rubie, D. C. (**1997**). "The cubic-tetragonal phase transition in the system majorite ($Mg_4Si_4O_{12}$) – pyrope ($Mg_3Al_2Si_3O_{12}$), and garnet symmetry in the Earth's transition zone," Phys. Chem. Miner. **24**, 206–221.

Hilton, E. (**2000**). *Composition and Structure of Titanian Andradite from Magmatic and Hydrothermal Environments* (University of British Columbia).

Larson, A. C. and Von Dreele, R. B. (**2000**). *General Structure Analysis System (GSAS).* (Report LAUR 86-748). Los Alamos National Laboratory.

Lee, P. L., Shu, D., Ramanathan, M., Preissner, C., Wang, J., Beno, M. A., Von Dreele, R. B., Ribaud, L., Kurtz, C., Antao, S. M., Jiao, X., and Toby, B. H. (**2008**). "A twelve-analyzer detector system for high-resolution powder diffraction," J. Synchrotron Radiat. **15**, 427–432.

Locock, A. J. (**2008**). "An excel spreadsheet to recast analyses of garnet into end-member components, and a synopsis of the crystal chemistry of natural silicate garnets," Comput. Geosci. **34**, 1769–1780.

Nakatsuka, A., Yoshiasa, A., Yamanaka, T., Ohtaka, O., Katsura, T., and Ito, E. (**1999**). "Symmetry change of majorite solid-solution in the system $Mg_3Al_2Si_3O_{12}$-$MgSiO_3$," Am. Mineral. **84**, 1135–1143.

Novak, G. A. and Gibbs, G. V. (**1971**). "The crystal chemistry of the silicate garnets," Am. Mineral. **56**, 1769–1780.

Otwinowski, Z. and Minor, W. (**1997**). "Processing of X-ray diffraction data collected in oscillation mode," In *Methods in Enzymology: Macromolecular Crystallography, part A, V. 276*, Eds. C.W. Carter, Jr. & R.M. Sweet, (Academic Press), pp. 307–326.

Parise, J. B., Wang, Y., Gwanmesia, G. D., Zhang, J., Sinelnikov, Y., Chmielowski, J., Weidner, D. J., and Liebermann, R. C. (**1996**). "The symmetry of garnets on the pyrope ($Mg_3Al_2Si_3O_{12}$) – majorite ($MgSiO_3$) join," Geophys. Res. Lett. **23**, 3799–3802.

Peterson, R. C., Locock, A. J., and Luth, R. W. (**1995**). "Positional disorder of oxygen in garnet: the crystal-structure refinement of schorlomite," Can. Mineral. **33**, 627–631.

Rietveld, H. M. (**1969**). "A profile refinement method for nuclear and magnetic structures," J. Appl. Crystallogr. **2**, 65–71.

Sacerdoti, M. and Passaglia, E. (**1985**). "The crystal structure of katoite and implications within the hydrogrossular group of minerals," Bull. Miner. **108**, 1–8.

Shannon, R. D. (**1976**). "Revised effective ionic radii and systematic studies of interatomic distances in halides and chalcogenides," Acta Crystallogr. **A32**, 751–767.

Sheldrick, G. M. (**1997**). SHELXL-97-1. Program for crystal structure determination. Institut für Anorg. Chemie, Univ. of Göttingen, Göttingen, Germany.
Shtukenberg, A. G., Popov, D. Y., and Punin, Y. O. (**2005**). "Growth ordering and anomalous birefringence in ugrandite garnets," Mineral. Mag. **69**, 537–550.
Smyth, J. R., Madel, R. E., McCormick, T. C., Munoz, J. L., and Rossman, G. R. (**1990**). "Crystal-structure refinement of a F-bearing spessartine garnet," Am. Mineral. **75**, 314–318.
Takéuchi, Y., Haga, N., Umizu, S., and Sato, G. (**1982**). "The derivative structure of silicate garnets in grandite," Z. Kristallogr. **158**, 53–99.
Toby, B. H. (**2001**). "EXPGUI, a graphical user interface for GSAS," J. Appl. Crystallogr. **34**, 210–213.
Wang, J., Toby, B. H., Lee, P. L., Ribaud, L., Antao, S. M., Kurtz, C., Ramanathan, M., Von Dreele, R. B., and Beno, M. A. (**2008**). "A dedicated powder diffraction beamline at the advanced photon source: commissioning and early operational results," Rev. Sci. Instrum. **79**, 085105.
Wildner, M. and Andrut, M. (**2001**). "The crystal chemistry of birefringent natural uvarovites: part II. Single-crystal X-ray structures," Am. Mineral. **86**, 1231–1251.

https://doi.org/10.1017/S0885715613001255 Published online by Cambridge University Press